Quantification of the local protein content in hydrogels undergoing swelling and dissolution at alkaline pH using fluorescence microscopy

Weiji Liu[a], D. Ian Wilson[b], Xiao Dong Chen[a], Ruben Mercadé-Prieto[a*]

[a] Suzhou Key Laboratory of Green Chemical Engineering, School of Chemical and Environmental Engineering, College of Chemistry, Chemical Engineering and Materials Science, Soochow University, Suzhou City, Jiangsu 215123, P.R. China

[b] Department of Chemical Engineering and Biotechnology, University of Cambridge, Philippa Fawcett Drive, Cambridge, CB3 OAS, UK

* Email: ruben@suda.edu.cn

Abstract:

Wide-field fluorescence microscopy was used to quantify the evolution of the volumetric swelling ratio, Q, *i.e.* solids content, in a protein hydrogel undergoing swelling and dissolution. Heat-induced whey protein hydrogels labelled with Rhodamine B isothiocyanate (RITC) were used as a model system. Complications in the quantification of Q using fluorescence of proteins conjugated RITC, arising from alkali destroying protein-dye interactions, were overcome using a reaction-diffusion numerical scheme. At pH 12-13, when the hydrogels dissolve readily, overlapping fluorescence intensity profiles were observed at different times, consistent with a system dissolving at steady state. In stronger alkali (*e.g.* 1 M NaOH), when dissolution proceeds very slowly, we confirm that there is little swelling next to the gel boundary. These results present the first quantification of the solids distribution within protein hydrogels under reactive conditions.

Key words: dissolution; Rhodamine B isothiocyanate; volumetric swelling ratio; whey protein hydrogels.

1. Introduction

The capability of globular proteins to form hydrogels when heated is exploited in the food industry in the manufacturing of functional products (Shewan and Stokes 2014), but is simultaneously unwelcome in food manufacturing processes where it can lead to extensive fouling, typically in heat exchangers (Blanpain-Avet et al. 2016), which is responsible for several industrial issues, such as heat exchange reduction due to an additional thermal resistance (Mahdi et al. 2009), high pressure drop owing to hydrodynamic diameter decrease (Grijspeerdt et al. 2004), and biocontaminations (Fryer et al. 2006).

Protein fouling deposits in industry are usually cleaned by the circulation of alkaline solutions in cleaning-in-place (CIP) operations (Alvarez et al. 2010). Despite the ubiquity of this cleaning problem, for example in the dairy industry where CIP is practiced on a daily basis, a coherent and quantitative understanding of the mechanisms involved is incomplete due to its complexity. For instance, protein gels swell when in contact with an alkaline solution: if the pH is high enough, both weak and strong chemical interactions are cleaved, allowing the hydrogels to swell further, rendering them weak so that erosion can occur and, eventually, dissolve (Mercadé-Prieto et al. 2008b). Extensive swelling has been suggested to help the removal of proteinaceous deposits as it allows small oligomers to diffuse through the swollen layer (Mercadé-Prieto et al. 2008b). Quantitative modelling of this process has been hampered, however, by the difficulty in quantifying, experimentally, the local spatial swelling ratio (or the protein concentration) of a hydrogel undergoing swelling or dissolution. Detailed mechanistic models for verification of the underlying science and optimization of CIP processes require such information.

The swelling behavior of hydrogels has been investigated both experimentally and theoretically (English et al. 1996; Ganji et al. 2010), as it often controls the release

behavior of solvents and drugs from polymeric networks (Ganji and Vasheghani-Farahani 2009; Lin and Metters 2006). Techniques that have been applied to assess the progression of swelling include X-ray microtomography (XμT; Laity et al. 2010; Laity and Cameron 2010), atomic force microscopy (AFM; Govedarica et al. 2012; Paredes et al. 2006), magnetic resonance imaging (MRI; Oztop et al. 2010; Richardson et al. 2005), or terahertz-pulsed imaging (TPI; Yassin et al. 2015). A review of these techniques has been presented by Huanbutta et al. (2013).

Fluorescence microscopy represents a cheaper alternative to the above techniques for obtaining this localised information. For instance, pyrene and dansyl dyes have been used to investigate the swelling and shrinking behavior of hydrogels using steady-state fluorescence as they are sensitive to the microenvironment, *i.e*. solvent polarity (Tari and Pekcan 2011). Raccis et al. (2011) employed fluorescence correlation spectroscopy to investigate the mobility of tracer molecules in a thermoresponsive hydrogel film. Quantitative studies are more challenging. Wagner et al. (2016) monitored the swelling and deswelling of polyacrylamide hydrogel using simultaneous neutron, fluorescence and optical brightfield transmission imaging. In a recent study we quantified the swelling of disc-shaped Rhodamine B isothiocyanate (RITC)-labelled whey protein hydrogels at pH ≤ 11 using a conventional wide-field fluorescence microscope (Liu et al. 2017). The results showed that the fluorescence intensity of the hydrogels decreased as expected for isotropic swelling at pH ≤11, when dissolution occurs very slowly, if at all.

In this paper we report the use of the same wide-field microscopy (WFM) technique to quantify, for the first time, the local swelling ratio of whey protein gels dissolving at higher pH. An important difference is the use of samples formed within narrow cuvettes (of cross-section 1 mm × 10 mm) rather than the discs employed by Liu et al. (2017) as this greatly helps in the identification of the gel-solution boundary and interpretation of fluorescence intensity data. A second aspect of technique development is the use of a model-based approach to account for changes in fluorescence intensity caused by breakdown of protein-dye interactions at higher pH.

2. Experimental procedure

2.1 Materials and gel preparation

The protocol to prepare RITC-labelled whey protein gels (denoted WPI-RITC) was reported previously (Liu et al. 2017). In brief, a 2 wt% solution of whey protein isolate (WPI; Davisco, USA) in MilliQ water was homogenized and mixed with 2% (v/v) RITC (Exciton, USA) stock solution (~20 mM). The pH of the solution was adjusted to 9 by adding 1 M NaOH (aq) to prevent protonation of the amine group without denaturing the protein (Taulier and Chalikian 2001). The solution was held at room temperature under mild stirring for at least 16.5 h to reach maximum labelling. Dialysis was then performed to remove the unreacted RITC aseptically using a 6-8 kDa MWCO membrane (Spectra Laboratories) against 0.02% (w/v) sodium azide solution. The concentration of WPI and of RITC inside the membrane was monitored by UV/Vis absorption at 280 nm and 555 nm, respectively (SpectraMax M5, Molecular Devices). Dialysis was normally stopped after 65 h, which typically resulted in a solution with concentrations of ~1.3 wt% WPI and ~0.1 mM RITC. The low dye-protein ratio was used to minimize the conformational changes of the protein due to labelling (Hungerford et al. 2007).

The protein concentration of the dialyzed solution is too low to form a gel, so native WPI powder was added to achieve a WPI concentration of 15 wt% with a final RITC concentration of ~20 µM. Heat-induced WPI-RITC hydrogels were formed by heating 400 µL aliquots of WPI-RITC solution inside glass cuvettes (dimensions 1 mm × 10 mm, 45 mm tall) in a water bath for 30 min at 80 °C. In order to minimize the formation of bubbles in the gel, solutions were degassed for at least 1 h at ~0.01 MPa and 40 °C before heat treatment. After cooling to room temperature the gels were stored at 4 °C overnight; they were allowed to equilibrate to room temperature for at least one hour before testing.

2.2 Swelling and dissolution of WPI-RITC gels

117

The swelling and dissolution of protein hydrogels prepared inside the cuvettes was studied at room temperature using similar protocols to those reported elsewhere (Mercadé-Prieto and Chen 2006). Each cuvette was immersed in a well-mixed solution at the desired pH at room temperature and removed at selected times for imaging. Imaging took 10 min or less, after which the cuvette was returned to the solution.

2.3 Fluorescence measurement with WFM

Fluorescence measurements were performed using the equipment and procedure reported by Liu et al. (2017). In brief, a wide-field fluorescence microscope (MacroZoom Z16, Leica) with a 1.0× planapochromatic objective (magnification 7.13× − 115×) was used. The RITC was excited at wavelength of 530 nm (520-550 nm band, LED4D067, Thorlabs) and its fluorescence emission was recorded as 8 bit images with a monochrome CCD camera (ICX285ALCCD, ToupTek, 1360×1024 pixels, chip size 6.45 µm).

The main area of interest in studying swelling and dissolution is the 'swollen layer' adjacent to the gel-solution boundary. Determining the location of this boundary using WFM is problematic because gels cannot be formed with flat perpendicular boundaries inside cuvettes, due to capillary forces promoting wall wetting (see Figure 1(b)). The cuvette surface could theoretically be coated to minimize the wall effect but this was not attempted here. As WFM can only provide reliable data when the gel thickness is known, the approach developed to estimate the location where the gel thickness is constant (*i.e.* where the gel fills the gap between the cuvette walls, denoted the constant gel thickness boundary, CGB), is explained below.

Figure 1(a) shows that the strong reflection at the gel interface when imaged dry, which affects the fluorescence intensity in this region, is avoided when the cuvette was submerged in a petri dish with water during imaging. The CGB is not visible in immersed images so the surface reflection in air was used to locate the CGB, using a high grey threshold value, as shown in Figure 1(*c*). It should be noted that the

147   immersion step generates an artefact when studying the gel in its initially formed state,

148   as the intensity at the boundary is slightly lower than that of the interior due to the

149   ingress of some water.

150   All images were obtained at the lowest magnification (*i.e.* 7.13×) to maximize the

151   field of view, typically needing 4 images to capture the length of the gel in the cuvette

152   (approximately 44 mm). Matlab$^{®}$ was used for image processing, including alignment,

153   image-merging and cropping of the 4 images (described in detail in Supplementary

154   Information, Figure S1). In order to minimize edge effects, only the central 8 mm region

155   of the gel was considered for analysis. Measurements were performed in darkness to

156   get high signal-to-noise ratios: the typical background noise was a grey value of ~0.23

157   per second of exposure time using an unlabeled WPI gel.

158

159   *2.4 Determination of the swelling ratio*

160

161   The overall volumetric swelling ratio, Q_o, defined as the reciprocal of the protein

162   volume fraction, $\phi_{2,s}$, was calculated from the total masses of the initial and the swollen

163   gel, m_0 and m_{sw}, respectively (Mercadé-Prieto et al. 2007a):

164     $$Q_o = \frac{1}{\phi_{2,s}} = 1 + \frac{\upsilon_{sp,1}}{\upsilon_{sp,2}}\left(\frac{1}{w}\frac{m_{sw}}{m_0} - 1\right) \tag{1}$$

165   where $\upsilon_{sp,1}$ and $\upsilon_{sp,2}$ are the specific volumes of the solvent (*i.e.* water) and the protein

166   (taken as 0.75×10^{-3} m^3 kg^{-1}) (Taulier and Chalikian 2001), respectively. w is the weight

167   fraction of protein in the initial gel. The value of Q_o at formation, calculated with m_{sw}

168     $= m_0$ and denoted Q_r, is used as the reference state.

169   Gel swelling is constrained in two dimensions by the cuvette walls. Assuming

170   constant gel density, width, thickness, dye stability and no dye leakage, the fluorescence

171   decrease due to 1D swelling is given by:

172     $$\frac{m_{sw}}{m_0} = \frac{V_{sw}}{V_0} = \frac{I_{WFM0}}{I_{WFM,sw}} \tag{2}$$

173   where I_{WFM0} and $I_{WFM,sw}$ are the fluorescence intensities of the initial and swollen gel,

174   respectively. Consequently, the local swelling ratio of the hydrogel, Q, can be calculated

175   from the local intensity via:

176 $$Q = 1 + \frac{\upsilon_{sp,1}}{\upsilon_{sp,2}} \left(\frac{1}{w} \left(\frac{I_{WFM,sw}}{I_{WFM0}} \right)^{-1} - 1 \right) \tag{3}$$

177

178 *2.5 Stability of WPI-RITC fluorescence in alkali*

179

180   The fluorescence intensity at a constant protein labelled RITC concentration of 7.5

181 µM was measured with addition of different native WPI concentrations, ranging from

182 0.75 to 15 wt%, at alkaline pH. As small volumes were used, the amount of NaOH (aq.)

183 required to achieve the desired pH was calculated using the hydrogen ion equilibrium

184 curve (Zhao et al. 2016). After mixing for 30 s, an aliquot was placed in a petri dish for

185 fluorescence measurements for 2.5 h. In control tests, MilliQ water was added instead

186 of alkali.

187

188 *2.6 Statistical Analysis*

189

190   The sigmoidal regressions were evaluated using the SigmaPlot v12.5 (Systat,

191 Software, Inc., USA). Welch t-tests were applied to check if fluorescence intensity

192 profiles were statistically the same.

193

194 **3. Results and Discussions**

195

196 *3.1 Initial protein gels*

197

198   Figure 2 shows the fluorescence profiles obtained for two gel samples before contact

199 with solution: the insets show the images after illumination correction (see Figure S2)

200 and image processing. Gel 1 contains some bubbles and water droplets whereas Gel 2

201 was free from such inhomogeneities. The gels were prepared using same degassing

202 protocol and demonstrates the need for care in preparing the gels.

203   Gel 2 shows homogeneous intensity except at the boundary, where a peak is evident.

204 The peak is generated by local dehydration at the boundary during storage, causing the

gel to shrink. In contrast, large fluctuations of the fluorescence intensity were observed in Gel 1 due to the bubbles and droplets. The two profile calculation methods show that the median value is more robust towards bubbles (see Figure S3: this supplementary Figure also shows that the variability in I_{WFM0}, from 12 repeats, was about 5%). The cuvettes are effectively identical (1.08 ± 0.01 mm thick) so this variation is attributed to small variations in RITC content between cuvettes and temperature fluctuations known to affect Rhodamine B fluorescence (Natrajan and Christensen 2009).

3.2 Velocity of the CGB during swelling and dissolution

The WFM technique allows the location of the CGB to be monitored and the velocity of this boundary, U_{BD}, to be estimated at different times. U_{BD} values for 15 wt% WPI-RITC gels submerged at different pH are plotted in Figure 3. Swelling (negative U_{BD}) is evident for all pH over the first ~1-2 h, changing to dissolution thereafter. The absolute value of U_{BD} decreases at pH 12-13, which is evident in the inset: these are also conditions which give rise to high dissolution rates (see Figure 4).

At longer times, U_{BD} approaches a roughly constant value, indicating that the dissolution rate is constant with time, which is consistent with many previous studies employing different techniques (Pérez-Mohedano et al. 2015). At high pH, U_{BD} decreases and is close to zero at pH 14, indicating an inhibited dissolution process. The constant dissolution rate velocities at pH 12-13 compare reasonably well with the penetration velocity of hydroxyl ion in BLG (*β*-lactoglobulin) or WPC (whey protein concentrate) gels reported previously (Mercadé-Prieto et al. 2008b; Mercadé-Prieto and Chen 2006). Figure 4 likewise shows that the estimated dissolution rates are in good agreement with directly measured rates reported previously.

3.3 Swelling at pH 11

Dissolution is slow at pH 11 and Figure 5 shows that extensive swelling is observed over a timescale of a few hours. In this case the experiment was terminated after 4.65

8

235 h as the CGB had emerged from the cuvette so swelling was no longer one dimensional.

236 The solids content in the gel near the CGB is so low that it is difficult to distinguish it

237 from the background. The images also show inhomogeneous swelling at the boundary,

238 driven by the wall layer, and the appearance of holes after 1.65 h, particularly when the

239 swelling is extensive (Figure S4). The effect of these defects was restricted by

240 considering only the central 8 mm band in the calculations and the median intensity.

241 The profiles in Figure 6(a) show uniform fluorescence intensity at the initial state,

242 with the CGB located about 8 mm from the cuvette entrance. The intensity does not

243 change over time in the gel fraction distant from the boundary (> 15 mm), consistent

244 with no ingress of solution there. These results demonstrate that the RITC-labelled gel

245 is sufficiently stable for reliable quantification.

246 Nearer the boundary the fluorescence intensity decreases as the gel swells. The

247 profiles show similar values in the region near the CGB boundary, up to ~2 mm deep,

248 which is confirmed in the insets where the data are plotted against depth into the gel.

249 Further into the gel, the intensity decreases steadily with time. The corresponding Q

250 values in Fig. 6(b) show high values at the CGB, decreasing to the initial value of ~9.4

251 in the unswollen region. These are all consistent with progressive swelling driven by

252 the diffusion of OH^- into the gel: these data represent the first direct measurements of

253 the dynamic response to immersion in alkali. The Q value at the CGB approaches a

254 steady value of 220 ± 40, which is in good agreement with the final Q_o value of ~200

255 obtained for disc-shaped gel samples (Liu et al. 2017).

256

257 3.4 *Fast dissolution (pH 12-13)*

258

259 Both the dissolution rate and the depth of penetration of OH^- into to the gel are known

260 to be constant with time at pH 12-13 (Mercadé-Prieto et al. 2008a), indicating that the

261 process is at steady state. The swollen layer is therefore expected to exhibit self-similar

262 profiles in fluorescence intensity (and Q). The profiles in Figure 7 show considerable

263 overlap and are statistically the same (p>0.05, Figure S5) despite there being extensive

264 dissolution, as indicated by U_{BD} in Figure 3 and the position of the CGB in the insets

in Figure 7. This is the first reported evidence confirming that when steady state dissolution occurs, the properties of the swollen layer are also constant. Furthermore, there is a noticeable and reproducible peak in the fluorescence intensity at the end of the inner limit of the swollen layer at pH $\geq$12.5, which is discussed later.

3.5 Fluorescence profiles at high pH (13.5-14)

At higher NaOH concentrations (pH > 13), at room temperature, the dissolution rate is known to decrease with time to very low values (Mercadé-Prieto and Chen 2006; Mercadé-Prieto et al. 2008b). Fluorescence intensity profiles at different times, such as those in Figure 8, did not show the overlap evident in Fig. 7. The limited dissolution at pH > 13 has been attributed to inhibition of swelling by the polyelectrolyte screening effect of the alkali (Mercadé-Prieto et al. 2007c). To date, only overall (macroscopic) swelling data have been available to support this hypothesis.

Mercadé-Prieto and Chen (2006) reported very low dissolution rates for WPC gels in 1 M NaOH. Mercadé-Prieto et al. (2007c) also reported low dissolution rates and little swelling for BLG hydrogels at high pH. Similar findings were obtained with these WPI-RTIC hydrogels (see Supplementary Figures S6 and S7). Therefore, the fluorescence intensity of gels at pH 14 was expected to be close to the initial value because the gels neither swelled nor dissolved. However, Figure 9 shows that the fluorescence intensity dropped dramatically and the affected region increased with time, indicating that the change in fluorescence is marking the volume exposed to alkali. Moreover, the quasi-linear profiles observed in the swollen layer at pH 12-13 (Fig. 7) have been replaced in Figures 8-9 by a strong decay, almost like a step function, indicating that the alkali is influencing the fluorescence of the WPI-RTIC gel. The approach to take into account this effect is described in the next section.

3.6 Quantifying the alkali effect on WPI-RITC fluorescence

The strong influence of pH on the fluorescence evident in Figure 9 was not expected

because the fluorescence of free Rhodamine B (RhB) in water is not affected at alkaline pH (Figure 10). The labelling of proteins with dyes is known to affect their quantum yield due to chemical or steric interactions (Chen 1969). In the current case, the quantum yield, or the fluorescence intensity at constant dye concentration, increases when RITC is covalently linked to whey proteins or in the presence of additional protein (Liu et al. 2017). It is postulated that at high pH these dye-protein interactions could be disrupted and thus lowering the quantum yield. Figure 10 shows that the fluorescence of the WPI-RITC conjugate, without added protein, decreases significantly at pH > 10.

The results in Fig. 10 were obtained at low protein concentrations, whereas in the gels the protein concentration is considerably higher. The effect of protein content on the decrease in fluorescence was studied in the WFM under dissolution-like conditions at constant WPI-RITC concentration. The fluorescence ratio, α, was defined as the ratio of values obtained under alkaline and neutral conditions. The average values of α over the first hour after mixing are plotted against pH in Figure 11. There is a sigmoidal decrease in α with pH between 9 and 13 which was fitted to the expression:

$$\alpha = \alpha_0 + \frac{\Delta\alpha}{1+\exp\left(\frac{p^*-pH}{\Delta p}\right)} \tag{4}$$

where α_0, $\Delta\alpha$, p^* and Δp are fitting parameters listed in Table 1. p^* corresponds to the pK of the transition, and occurs at ~11.6. This value provides insight into why the fluorescence of the WPI-RITC gels decrease with pH: similar pK values were observed in the alkaline denaturation of BLG aggregates (Mercadé-Prieto et al. 2007b), and both values are higher than that reported for the base denaturation of unaggregated BLG, at pH ~10.6 (Taulier and Chalikian 2001). The pK shift in BLG was caused by non-covalent interactions between protein aggregates, and we suggest that similar dye-protein interactions are destroyed here, thereby decreasing the fluorescence intensity.

The results for 10 wt% WPI in Figure 11 differ from the other data sets. Table 1 shows that its $\Delta\alpha$ term is significantly different to the other values. The trends were reproducible, but it was decided to exclude this set from subsequent calculations to

324 correct the fluorescence data for simplicity. The difference between the values of α at
325 10 wt% WPI calculated by interpolation (using the sigmoid function parameters from
326 other [WPI] conditions) and the simulated values (using the sigmoid regression
327 parameters at 10 wt%) were used to quantify the uncertainty in α at [WPI] between 5
328 and 15 wt% (11 < pH < 13), resulting with an average relative error of α ~20%.

329 Above pH 13 the α values decrease further, in a linear manner that cannot be readily
330 represented by the sigmoidal expression (Eqn. (4)): α was therefore calculated using
331 linear interpolation in the interval pH 13-14. The variability of α values at the same pH
332 for different [WPI] is considered as the uncertainty in α with an average absolute error
333 of 0.024. Alkaline induced gelation could occur during the fluorescence measurements,
334 especially when the [WPI] was high (e.g. 15 wt%), but no significant influence of this
335 sol-gel transition on the fluorescence was evident. The fluorescence intensity can also
336 depend weakly on the reaction time (results not presented) and this is accounted for by
337 determining average α values within one hour of contact with alkali. This was
338 considered reasonable as the residence time of the OH$^-$ within the gel before the gel
339 dissolves completely is less than one hour at pH 12-13.

340

341 3.7 *Estimation of pH within gels*

342

343 Since the aim of this study was to use fluorescence techniques to quantify the local
344 protein content in the swollen gel layer during dissolution, and Fig. 11 shows that
345 fluorescence is strongly affected by both pH and [WPI], the following scheme was
346 devised to account for these effects.

347 Knowledge of the local pH is required to calculate α but this has not yet been
348 measured inside a dissolving gel. The pH inside the gel was estimated numerically
349 using the Fickian diffusion model for NaOH through protein gels presented by
350 Mercadé-Prieto et al. (2008a), which considers consumption of the alkali due to the
351 titration of the proteins as well as dissolution. A summary of the model is given in the
352 Appendix. The model does not consider changes in the protein concentration - [WPI]
353 is held at the initial value of 15 wt% - so the estimate of the local pH is likely to be poor

354 when there is substantial swelling. More reliable values are expected at pH 14, when

355 both swelling and dissolution are limited but there is extensive diffusion of OH$^-$ within

356 the gel.

357 Figure 12(a) shows the pH profiles calculated by the model for cases where the

358 dissolution rate is constant, with bulk solution pH 12-13. The calculations employed an

359 effective diffusivity, D_{eff}, of 1.7×10^{-9} m^2 s^{-1} and a constant NaOH penetration thickness

360 with time (δ_{OH}). Both parameters were obtained from the literature for BLG gels using

361 phenolphthalein to visualize the penetration of NaOH at pH $\geq$ 9.8 (Mercadé-Prieto et

362 al. 2008a). The plots show that the pH changes noticeably within the swollen layer, and

363 values are high as expected, so that correction of α with pH is certainly required when

364 estimating Q.

365 For pH > 13, the dissolution rate is not constant, and therefore δ_{OH} is not constant

366 either. The model was modified to include an initial period in which there was no

367 dissolution (*e.g.* 1 hour in Figure 13(b)). In this initial phase the sharp decrease in

368 fluorescence intensity evident in Fig. 8 and 9 should be related to a region where α

369 decreases markedly due to pH, *i.e.* near the pK at pH 11-12. Inspection of the pH and

370 fluorescence profiles shows this to be the case in Figures 12(b) and (c).

371 If it is assumed that the steep decrease in fluorescence far from the CGB at pH 13.5

372 and 14 is only due to pH, e.g. the protein concentration is approximately 15 wt% as

373 there has been little time for dissolution to occur, then the local pH in that part of the

374 gel can be estimated. The results are plotted as dotted lines in Fig.13(b) and (c). The

375 model parameters, mainly D_{eff}, can be determined from the data, and were adjusted in

376 order to obtain similar pH profiles to the dotted lines. The D_{eff} values obtained, ranging

377 from $1.5\text{-}1.7 \times 10^{-9}$ m^2 s^{-1}, are in good agreement with previous studies on BLG gels

378 (Mercadé-Prieto et al. 2008a). These results provide confidence in the prediction of

379 local pH for determining α and thus Q.

380

381 *3.8 Corrected Q profiles in gels at high pH*

382

383 Once the pH profiles within the gel had been obtained, an estimate of the local protein

384 concentration in the gel is also required in order to calculate the fluorescence correction

385 factor (i.e. α). This was done by solving eq. (3) and (4) iteratively, starting with an

386 initial estimate of [WPI] of 1 wt%. The corrected fluorescence intensity profiles at pH

387 12-13 are presented in Figure 13(*a*), for locations where the estimated pH was > 11.5.

388 The fluorescence intensity values are now considerably higher (compare with Fig. 7).

389 The Q values were calculated (see insets) and close to the CGB the values were 110 $\pm$

390 20, 25 $\pm$ 8 and 11 $\pm$ 2 for pH 12, 12.5 and 13, respectively. The corresponding [WPI]

391 values at the interface were 1.3 $\pm$ 0.2, 5.6 $\pm$ 1.7 and 13 $\pm$ 3 wt% (Figure S8). The

392 uncertainties reported consider both the repeatability in I_{WFM} and the uncertainty in α.

393 Previous research has shown that if the pH is high enough (in practice, between pH

394 11-12) (Mercadé-Prieto et al. 2007b), and if gels swell above a certain extent,

395 macroscopic dissolution will readily occur, termed 'dissolution threshold' behavior

396 (Mercadé-Prieto et al. 2007a). Critical Q values below which macroscopic gels are

397 stable during swelling experiments were estimated at about 23 for similar WPI gels (Li

398 et al. 2016), and around 17 for BLG gels (Mercadé-Prieto et al. 2007a). The Q values

399 near the CGB at pH 12 in Figure 13(*a*) are much higher than these but the values at pH

400 12.5 and 13 are reasonably similar. The existence of a swollen layer with Q greater than

401 the critical value at pH 12 and pH 12.5 is possible as dissolution occurs relatively slowly

402 (Fig. 4). The thickness of the high Q region is ~0.7 mm at pH 12 and ~0.1 mm at pH

403 12.5. At pH 13, when dissolution occurs more quickly, the region is very thin and Q at

404 the boundary Q is close to the critical value.

405 Figure 13(*b*) shows that at pH 13.5, the corrected fluorescence intensity profiles are

406 statistically the same to that of the initial state (p>0.05, Fig. S9(a)), implying limited

407 swelling, with some swelling occurring at the boundary in the subsequent 2 h. At pH

408 14 (Figure 13(*c*)), where there is little swelling and dissolution, the fluorescence

409 intensity inside the gels remain fairly constant (p>0.05, Fig. S9(b)). The average value

410 of Q at different times for pH 13.5 is similar (11 $\pm$ 2) to the Q value for pH 13. At pH

411 14, the average value of Q at different times (16 $\pm$ 3) is in good agreement with the

412 value of ~15 reported from macroscopic swelling experiments (Li et al. 2016).

413 These results demonstrate the capability of WFM to measure Q locally in a protein

hydrogel undergoing dissolution and swelling. This is not possible using classical gravimetric or volumetric methods. The pH and the [WPI] dependence of the WPI-RITC fluorescence presents a real challenge for accurate quantification, not only in the determination of the correction factor α, but also in the estimation of the pH inside the gel. For instance, the uncertainty in the intragel pH, which has not been considered here, is affected by the modeling assumption that the [WPI] is constant during the diffusion of NaOH. If the lower [WPI] estimated here were used, faster NaOH diffusion is expected (e.g. less titration reactions and higher diffusivity at lower [WPI]), resulting in slightly higher intragel pH. Therefore, due to α, higher Q values should be expected inside the swollen layer, particularly at pH 12-13 (Fig. 13(a)). Close to the gel boundary, where the estimated pH is similar to that of the solutions, Q corrections should be minimal. Accurate intragel pH estimations, however, will be only possible if local pH experimental data is ever available.

More reliable estimates with fluorescence techniques will require dye-protein conjugates not affected at the high pHs encountered in cleaning and dissolution studies. It may be noted that a correction was not applied for the swelling-only experiment at pH 11 (Fig. 6). The fluorescence corrections are small at lower pH and low [WPI], as shown in Fig.11. This is confirmed by the integrated fluorescence remaining almost unchanged over the length of the swelling experiment (Fig. S10).

3.9 *Estimated NaOH penetration depth, δ*

The diffusion of OH⁻ ions is critical in the dissolution of fouling deposits or gels due to their ability to destroy the gel matrix and solubilize proteins (Christian and Fryer 2006). Mercadé-Prieto et al. (2008a) used phenolphthalein to track the diffusion of NaOH into BLG gels as it changes color when pH > 9.8. In our case, the above results reveal a strong alkali effect on the conjugated RITC fluorescence, suggesting that the NaOH penetration depth, δ, could be measured using uncorrected fluorescence intensity profiles. Figure 14 shows schematics of three ways that WFM could be used to

444   determine δ.

445   In Figure 14(*a*) measure δ_1 is the distance between the CGB (determined from

446   bright light microscopy) and the marked point (L_1^*), where the fluorescence intensity

447   is equal to the initial value (*i.e.* I_{WFM0}). The location of L_1^* was obtained by spline

448   interpolation. Figure 14(*b*) shows the scenario at pH 12.5-14 where a fluorescence peak

449   exists close to the alkali penetration front. Measures δ_2 and δ_3 are the distance between

450   the CGB and the points where the fluorescence intensity is equal to the initial value,

451   located before (L_2^*) or after (L_3^*) the fluorescence peak, respectively.

452   Figure 15 shows how the NaOH penetration depth measured thus changes with time.

453   At pH 12-13, constant values of δ are observed for both δ_2 and δ_3: this is the regime

454   when the gel dissolves at a constant rate, while at other conditions δ increases

455   continuously with time, with coincidentally similar values observed for pH 11 and 14.

456   The δ_2 values at pH 12.5 and 13 are consistent with those reported for BLG gels

457   visualized by phenolphthalein (i.e. δ_{OH}) (Mercadé-Prieto et al. 2008a), however, much

458   larger values of δ_2 are observed at pH 12. This consistency between δ and δ_{OH}

459   strengthens the confidence in the simulated NaOH concentration results, where δ_{OH} was

460   an input parameter in the calculation (Section 3.7).

461   The above results indicate that the alkaline pH at the fluorescence peak is relatively

462   low (say pH < 10). An unexpected fluorescence peak was also observed during swelling

463   in disc-shaped WPI-RITC gels (Liu et al. 2017). As this peak was only observed when

464   fast swelling occurred, it could be related to anomalous water transport in the gel

465   interior, i.e. shrinkage, decreasing Q. Considering the complex effects of pH and protein

466   concentration on RITC-WPI fluorescence reported above, it is not possible at this stage

467   to exclude that the feature was caused by changes in the quantum yield of the conjugate.

468

469   **4. Conclusions**

470   Wide-field fluorescence microscopy (WFM) has been used to quantify the

471   volumetric swelling ratio Q, e.g. protein content, in hydrogels undergoing swelling and

472   dissolution at room temperature. The hydrogels dissolve readily at pH 12-13, reaching

473   a steady state which is confirmed by the local variation in Q and the size of the swollen

474   layer. Under strongly alkaline conditions (e.g. pH 14), when dissolution proceeds very

475   slowly, we confirm experimentally that there is very little swelling, which could be the

476   reason for the inhibited dissolution suggested in previous studies. This result might

477   explain why there is an optimum for the cleaning of diary fouling deposits using alkali.

478   The WFM measurements showed that the highly alkaline conditions cause

479   breakdown of dye-protein interactions that affect the fluorescence of whey proteins

480   conjugated with RITC. A scheme for correcting the effects of alkali and protein

481   concentration was devised and shown to give reasonable results. This allowed us to

482   quantify the protein content within these protein hydrogels under reactive conditions

483   for, to the authors' knowledge, the first time. In addition, we attempt to apply this

484   approach to monitor *in situ* the growth of fouled layer on the surface of heat exchanger

485   in the future, and hopefully to build a quantitative model as well.

486

487

488

489

490

491   **APPENDIX**

492

493   The NaOH concentration profile in a gel is estimated using Fick's first law combined

494   with conservation of mass as reported by Mercadé-Prieto et al. (2008a). This requires

495   numerical evaluation, with length (h) and time intervals (Δt) satisfying

496    $\frac{D_{\text{eff}}\Delta t}{h^2} = 0.5$ (eq. A1)

497   where D_{eff} is the effective diffusivity of NaOH in the gel. The NaOH concentration at a

498   specific depth x and at time $t' = t+\Delta t$ can be estimated from the previous time interval,

499   denoted t, using

500    $[OH^-]_{x,t+\Delta t}=0.5([OH^-]_{x-h,t} +[OH^-]_{x+h,t})$ (eq. A2)

501   During each time interval Δt, the final NaOH concentration that remained in the

502   gel is corrected considering the consumption of acid-base reactions with ionizable

503   amino acids. The amount of NaOH consumed can be calculated from:

504    $[\text{OH}^-]_{x,t+\Delta t} - [\text{OH}^-]^C_{x,t+\Delta t} = [\text{WPI}]_{x,t+\Delta t} \sum_k \text{N}_k \left(\frac{1}{1+\text{K}_{b,k}[\text{OH}^-]^C_{x,t}} - \frac{1}{1+\text{K}_{b,k}[\text{OH}^-]^C_{x+\Delta t}} \right)$ (eq. A3)

505   where the $[\text{OH}]^C_{x,t+\Delta t}$ is the corrected final NaOH concentration at position x and time

506    $t+\Delta t$. The protein concentration, $[\text{WPI}]_{x,t+\Delta t}$, is calculated considering whey protein as

507   pure β-lactoglobulin (18.4 kDa). The subscript k corresponds to each of the different

508   ionizable residues on the protein at alkaline pH (*i.e.* His, Tyr, Lys, Arg), N_k is the number

509   of units of amino acid k on the protein, and $K_{b,k}$ is the basicity constant for the side

510   chain. The values used in this work were those reported by (Zhao et al. (2016)).

511

512   **Acknowledgements**

519

520   **References**

521

522   Alvarez N, Daufin G & Gésan-Guiziou G (2010) Recommendations for rationalizing cleaning-in-place in
523   the dairy industry: Case study of an ultra-high temperature heat exchanger. Journal of Dairy
524   Science. 93(2), 808-821.
525   Blanpain-Avet P, Andre C, Khaldi M, Bouvier L, Petit J, Six T, Jeantet R, Croguennec T & Delaplace G (2016)
526   Predicting the distribution of whey protein fouling in a plate heat exchanger using the kinetic
527   parameters of the thermal denaturation reaction of beta-lactoglobulin and the bulk
528   temperature profiles. Journal of Dairy Science. 99(12), 9611-9630.
529   Chen RF (1969) Fluorescent protein-dye conjugates : II. Gamma globulin conjugated with various dyes.
530   Archives of Biochemistry & Biophysics. 133(2), 263-276.
531   Christian GK & Fryer PJ (2006) The Effect of Pulsing Cleaning Chemicals on the Cleaning of Whey Protein
532   Deposits. Food and Bioproducts Processing. 84(4), 320-328.
533   English AE, Mafé S, Manzanares JA, Yu X, Grosberg AY & Tanaka T (1996) Equilibrium swelling properties
534   of polyampholytic hydrogels. Journal of Chemical Physics. 104(21), 8713-8720.
535   Fryer PJ, Christian GK & Liu W (2006) How hygiene happens: Physics and chemistry of cleaning.
536   International Journal of Dairy Technology. 59(2), 76-84.

537   Ganji F & Vasheghani-Farahani E (2009) Hydrogels in Controlled Drug Delivery Systems. Iranian Polymer
538   Journal. 18(1), 63-88.

539   Ganji F, Vasheghani-Farahani S & Vasheghani-Farahani E (2010) Theoretical Description of Hydrogel
540   Swelling: A Review. Iranian Polymer Journal. 19(5), 375-398.

541   Govedarica B, Sovany T, Pintye-Hodi K, Skarabot M, Baumgartner S, Musevic I & Srcic S (2012) Addressing
542   potent single molecule AFM study in prediction of swelling and dissolution rate in polymer
543   matrix tablets. European Journal of Pharmaceutics and Biopharmaceutics. 80(1), 217-225.

544   Grijspeerdt K, Mortier L, De Block J & Van Renterghem R (2004) Applications of modelling to optimise
545   ultra high temperature milk heat exchangers with respect to fouling. Food Control. 15(2), 117-
546   130.

547   Huanbutta K, Terada K, Sriamornsak P & Nunthanid J (2013) Advanced technologies for assessment of
548   polymer swelling and erosion behaviors in pharmaceutical aspect. European Journal of
549   Pharmaceutics and Biopharmaceutics. 83(3), 315-321.

550   Hungerford G, Benesch J, Mano JF & Reis RL (2007) Effect of the labelling ratio on the photophysics of
551   fluorescein isothiocyanate (FITC) conjugated to bovine serum albumin. Photochemical &
552   Photobiological Sciences Official Journal of the European Photochemistry Association & the
553   European Society for Photobiology. 6(2), 152-158.

554   Laity PR & Cameron RE (2010) Synchrotron X-ray microtomographic study of tablet swelling. European
555   Journal of Pharmaceutics and Biopharmaceutics. 75(2), 263-276.

556   Laity PR, Mantle MD, Gladden LF & Cameron RE (2010) Magnetic resonance imaging and X-ray
557   microtomography studies of a gel-forming tablet formulation. European Journal of
558   Pharmaceutics and Biopharmaceutics. 74(1), 109-119.

559   Li H, Zhao L, Chen XD & Mercadé-Prieto R (2016) Swelling of whey and egg white protein hydrogels with
560   stranded and particulate microstructures. International Journal of Biological Macromolecules.
561   83, 152-159.

562   Lin C-C & Metters AT (2006) Hydrogels in controlled release formulations: Network design and
563   mathematical modeling. Adv Drug Deliv Rev. 58(12–13), 1379-1408.

564   Liu WJ, Chen XD & Mercadé-Prieto R (2017) Spatial quantification of hydrogels swelling using wide-field
565   fluorescence microscopy. Chemical Engineering Science. 158, 349-358.

566   Mahdi Y, Mouheb A & Oufer L (2009) A dynamic model for milk fouling in a plate heat exchanger. Applied
567   Mathematical Modelling. 33(2), 648-662.

568   Mercadé-Prieto R & Chen XD (2006) Dissolution of whey protein concentrate gels in alkali. AIChE Journal.
569   52(2), 792-803.

570   Mercadé-Prieto R, Falconer RJ, Paterson WR & Wilson DI (2007a) Swelling and dissolution of beta-
571   lactoglobulin gels in alkali. Biomacromolecules. 8(2), 469-476.

572   Mercadé-Prieto R, Paterson WR, Chen XD & Wilson DI (2008a) Diffusion of NaOH into a protein gel.
573   Chemical Engineering Science. 63(10), 2763-2772.

574   Mercadé-Prieto R, Paterson WR & Wilson DI (2007b) The pH threshold in the dissolution of beta-
575   lactoglobulin gels and aggregates in alkali. Biomacromolecules. 8(4), 1162-1170.

576   Mercadé-Prieto R, Sahoo PK, Falconer RJ, Paterson WR & Wilson DI (2007c) Polyelectrolyte screening
577   effects on the dissolution of whey protein gels at high pH conditions. Food Hydrocolloids. 21(8),
578   1275-1284.

579   Mercadé-Prieto R, Wilson DI & Paterson WR (2008b) Effect of the NaOH Concentration and Temperature
580   on the Dissolution Mechanisms of ß-Lactoglobulin Gels in Alkali. International Journal of Food

581   Engineering. 4(5), 284-290.

582 Natrajan VK & Christensen KT (2009) Two-color laser-induced fluorescent thermometry for microfluidic
583   systems. Measurement Science and Technology. 20(1), 015401.

584 Oztop MH, Rosenberg M, Rosenberg Y, Mccarthy KL & Mccarthy MJ (2010) Magnetic Resonance Imaging
585   (MRI) and Relaxation Spectrum Analysis as Methods to Investigate Swelling in Whey Protein
586   Gels. Journal of Food Science. 75(75), 508-515.

587 Pérez-Mohedano R, Letzelter N & Bakalis S (2015) Development of a swelling-removal model for the
588   scanning fluid dynamic gauge. Food and Bioproducts Processing. 93, 269-282.

589 Paredes JI, Villar-Rodil S, Tamargo-Martínez K, Martínez-Alonso A & Tascón JMD (2006) Real-Time
590   Monitoring of Polymer Swelling on the Nanometer Scale by Atomic Force Microscopy. Langmuir.
591   22(10), 4728-4733.

592 Raccis R, Roskamp R, Hopp I, Menges B, Koynov K, Jonas U, Knoll W, Butt HJ & Fytas G (2011) Probing
593   mobility and structural inhomogeneities in grafted hydrogel films by fluorescence correlation
594   spectroscopy. Soft Matter. 7(15), 7042-7053.

595 Richardson JC, Bowtell RW, Mader K & Melia CD (2005) Pharmaceutical applications of magnetic
596   resonance imaging (MRI). Adv Drug Deliv Rev. 57(8), 1191-1209.

597 Shewan HM & Stokes JR (2014) Review of techniques to manufacture micro-hydrogel particles for the
598   food industry and their applications. Journal of Food Engineering. 119(4), 781-792.

599 Tari O & Pekcan O (2011) Modelling of Swelling by the Fluorescence Technique in Kappa Carrageenan
600   Gels. AIP Conference Proceedings. 1400(1), 470-475.

601 Taulier N & Chalikian TV (2001) Characterization of pH-induced transitions of β-lactoglobulin: ultrasonic,
602   densimetric, and spectroscopic studies. Journal of Molecular Biology. 314(4), 873-889.

603 Wagner D, Burbach J, Grünzweig C, Hartmann S, Lehmann E, Egelhaaf SU & Hermes HE (2016) Solvent
604   and solute ingress into hydrogels resolved by a combination of imaging techniques. The Journal
605   of Chemical Physics. 144(20), 204903.

606 Yassin S, Su K, Lin H, Gladden LF & Axel Zeitler J (2015) Diffusion and Swelling Measurements in
607   Pharmaceutical Powder Compacts Using Terahertz Pulsed Imaging. J Pharm Sci. 104(5), 1658-
608   1667.

609 Zhao L, Chen XD & Mercadé-Prieto R (2016) Understanding the alkali cold gelation of whey proteins
610   with NaCl and SDS. Rheologica Acta. 55(11-12), 909-920.

611

612

613

614
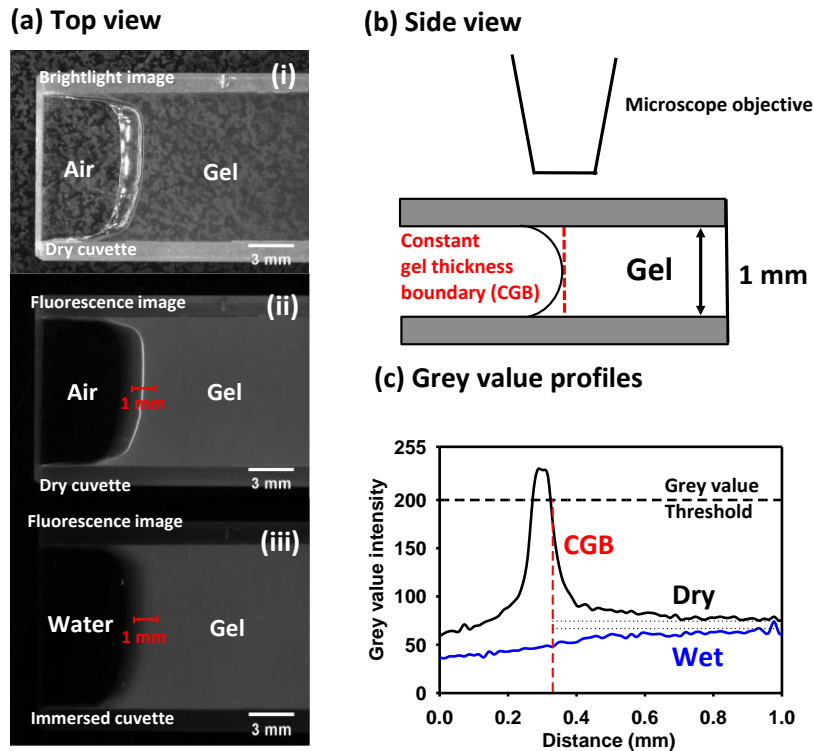
Figure 1. WFM methodology. (*a*) Images of a 15 wt% WPI-RITC gel after gelation: (*i*) bright light, (*ii*) fluorescence, in air, exposure time 8 s, (*iii*) fluorescence, submerged in water, exposure time 8 s; (*b*) Schematic of gel formed in cuvette showing curved boundaries region at wall – dashed vertical line denotes the location of the CGB; (*c*) Variation in grey intensity values along the lines marked in (*a*): Horizontal dotted lines indicate the fluorescence intensity recorded in the interior of the gel, distant from the boundary; black dashed line shows the threshold value applied to a dry image to locate the CGB in an immersed image.

623

624
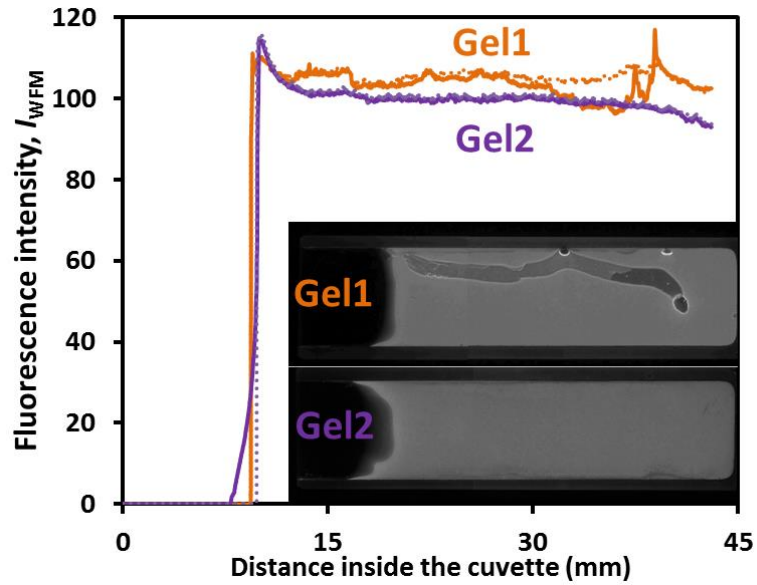
Figure 2. Profiles of 1-D fluorescence intensity for 15 wt% WPI-RITC gels after formation. The fluorescence intensity at each location is calculated using the mean grey value (continuous line) and median grey value (dashed line) of the whole width of the gel as outlined in text. Image acquisition condition: magnification 7.13×; exposure time 8 s; pixel size ~14 μm.

630

631

632
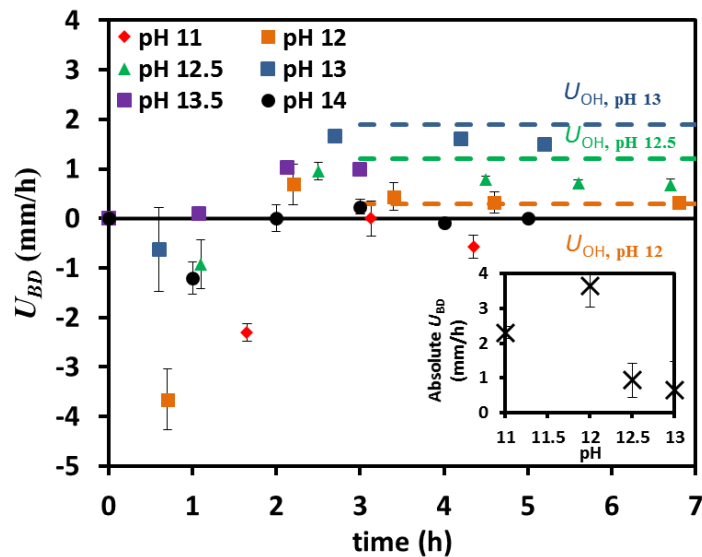
Figure 3. Evolution of gel boundary (CBD) velocity for 15 wt% WPI-RITC hydrogels at different pH. Horizontal dashed lines denote the penetration velocity of NaOH into

635   β-lactoglobulin (BLG) gels, U_{OH}, reported by Mercadé-Prieto et al. (2008a). Inset

636   shows the absolute U_{BD} during the initial swelling period (1-2 h). Error bars are the

637   standard deviation (SD) of triplicate experiments.

638
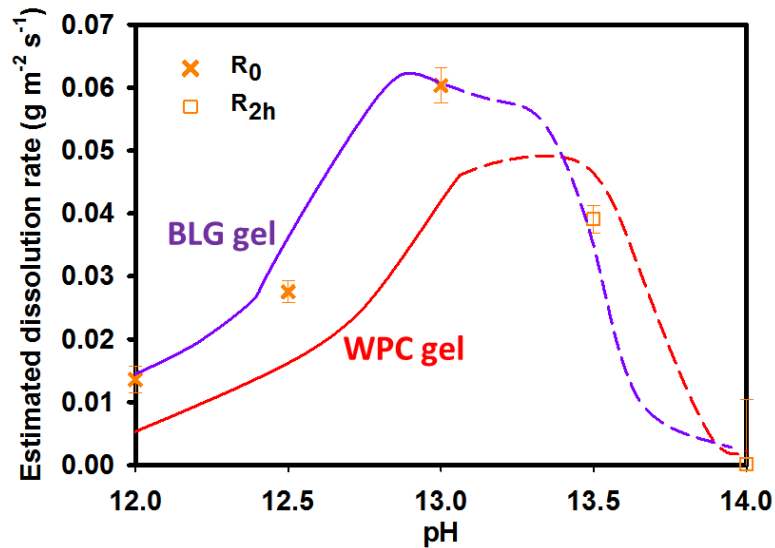
639

640

641   **Figure 4**. Comparison of dissolution rates estimated from U_{BD} data for the WPI-RTIC

642   hydrogels with those reported for whey protein concentrate (WPC) (Mercadé-Prieto

643   and Chen 2006), and β-lactoglobulin (BLG) gels (Mercadé-Prieto et al. 2008b). R_0

644   (solid loci) denotes constant dissolution rates, calculated for experiments where a

645   constant U_{BD} was reached; R_{2h} values (dashed loci) are rates calculated for other cases

646   after 2 h of dissolution, as the rates are not constant with time. Error bars as in Fig. 3.
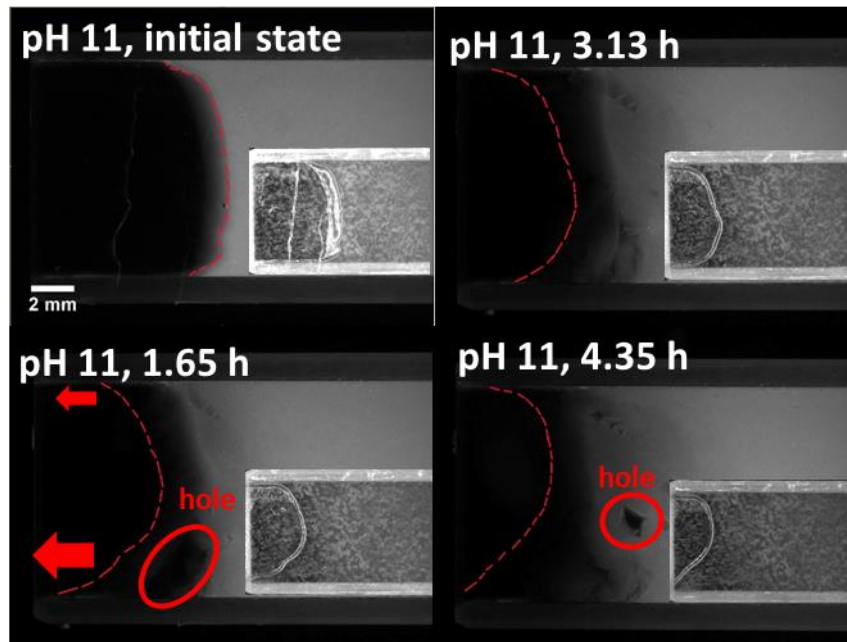
Figure 5. Top view of gels swelling after extended contact at pH 11. Exposure time: 8 s. Insets show bright line images obtained under dry conditions. Red dashed lines denote the estimated CGB location. Length scale common to all frames.
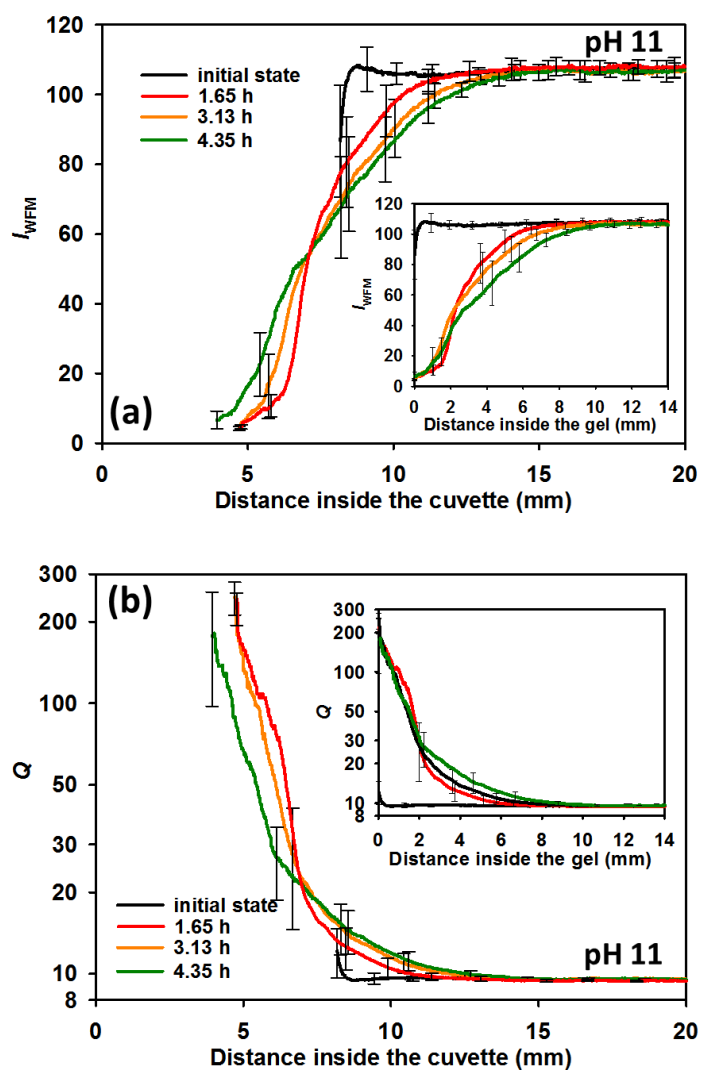
Figure 6. Profiles of (*a*) fluorescence intensity, and (*b*) corresponding local swelling ratio for 15 wt% WPI-RITC hydrogels swelling at pH 11. *Q* was calculated using eq. 3. Error bars show SD of triplicates. Insets show the data plotted against distance from CGB. Note the logarithmic scale for *Q* in (*b*).

652

653

654

655

656

657
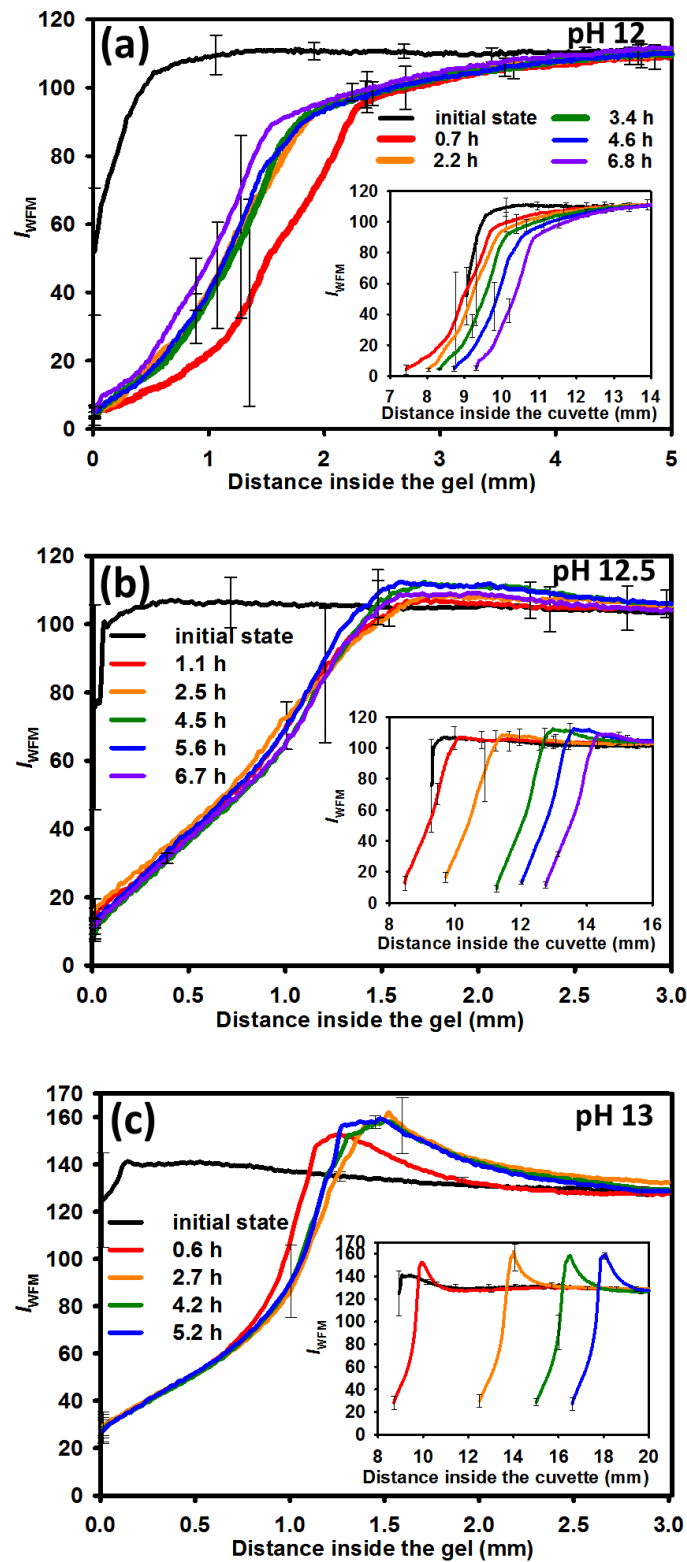
Figure 7. Fluorescence intensity profiles obtained at (*a*) pH 12, (*b*) pH 12.5, and (*c*) pH 13 at different times. Insets show profiles relative to cuvette entrance. Error bars indicate SD of three repeated experiments.

26

663

664
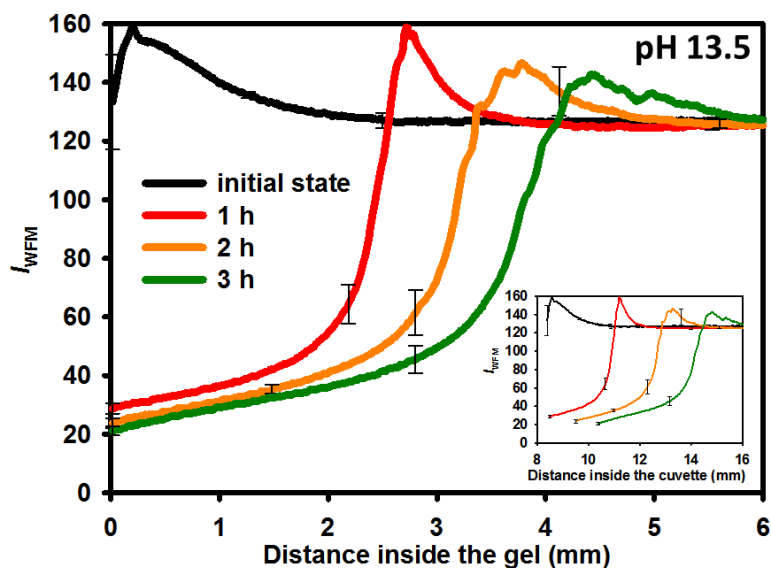
Figure 8. Fluorescence profiles obtained for hydrogels exposed to NaOH solution at pH 13.5 at different times (see legend). Error bars indicate the SD of triplicates. Inset shows fluorescence profiles against distance from the cuvette entrance.

668

669

670
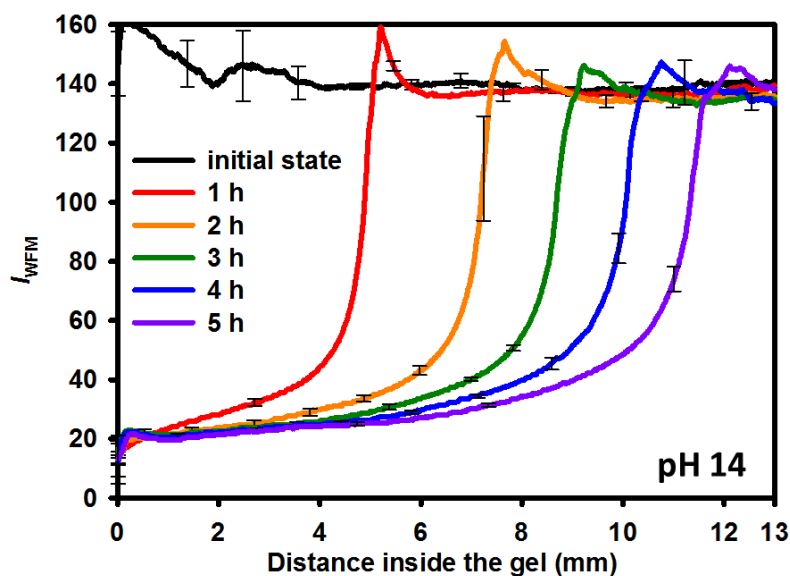
Figure 9. Fluorescence profiles of 15 wt% WPI-RITC hydrogels exposed to NaOH solution at pH 14 for different times (see legend). Error bars show the SD of three repeated experiments.
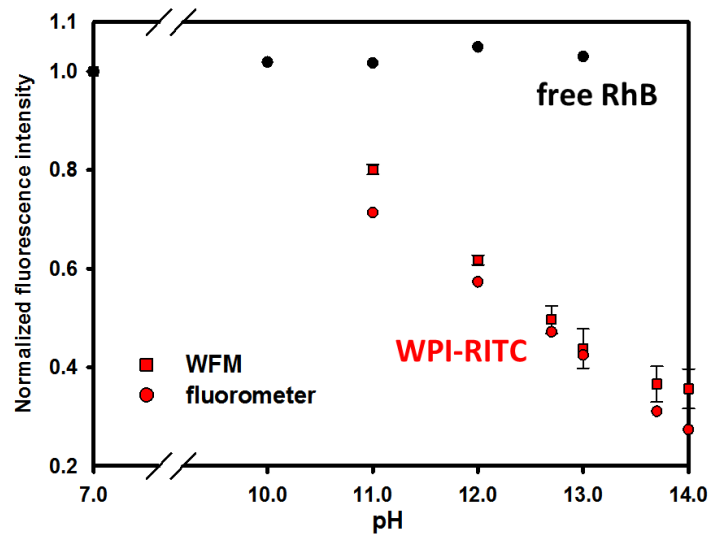
Figure 10. Effect of pH on the normalized fluorescence intensity of free RhB and WPI-RITC conjugates. The fluorescence of WPI-RITC was obtained using a fluorometer and by WFM. Fluorometer measurement conditions: excitation 530 nm; emission 580 nm. Error bars for WFM show the SD using three magnifications.
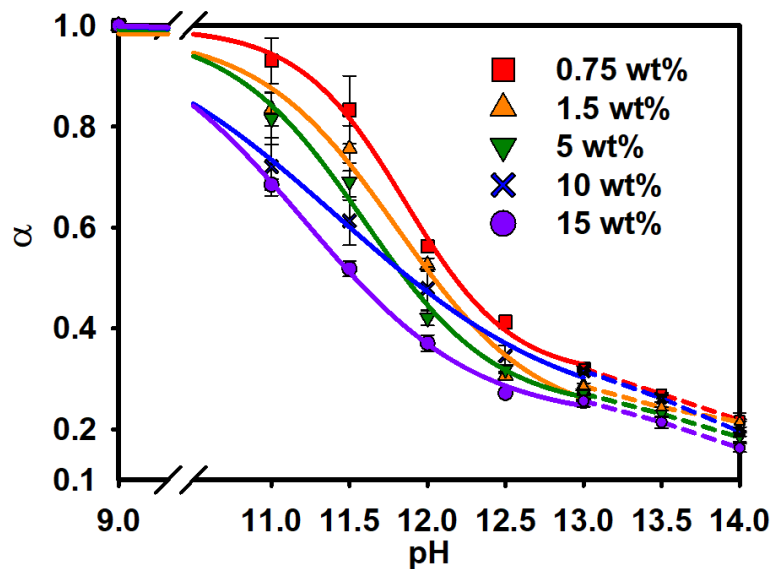

Figure 11. Effect of pH on fluorescence ratio α at different native WPI concentrations (shown in legend). Error bars show SDs of α within the first hour of mixing with alkali;

685   for the case of 10 wt% two data sets were used. Solid lines show sigmoidal fit of data

686   to Eq. (4); regression parameters are reported in Table 1. Dotted lines at pH 13-14

687   denote α values estimated by linear interpolation.

688

689

690
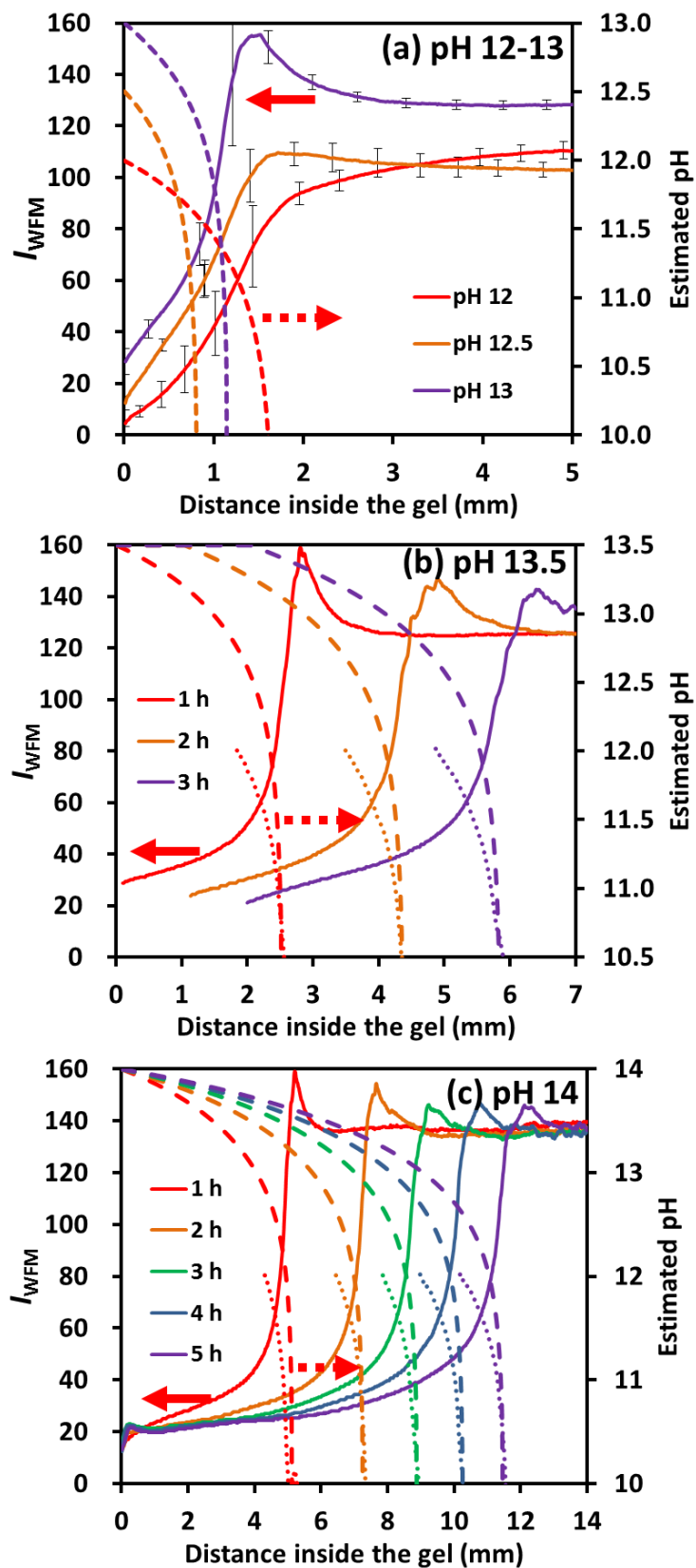
Figure 12. Estimated pH profiles and corresponding experimental fluorescence intensity profiles, for 15 wt% WPI-RTIC gels dissolving in NaOH at pH (*a*) 12-13, (*b*)

693　13.5 and (*c*) 14. The profiles in (*a*) are for steady state conditions, whereas those in (*b*)

694　and (*c*) change over time. Error bars in (*a*) show SDs of overlapping profiles in triplicate

695　experiments. Simulation parameters: (*a*) $D_{eff} = 1.7 \times 10^{-9}\,\text{m}^2\,\text{s}^{-1}$: constant dissolution, δ_{OH}

696　$= 1.6, 0.8$ and 1.15 mm, for pH 12, 12.5 and 13, respectively (Mercadé-Prieto et al.

697　2008a). (*b*) No dissolution during the first hour, with $D_{eff} = 0.8 \times 10^{-9}\,\text{m}^2\,\text{s}^{-1}$, followed by

698　uniform dissolution at a rate of 0.017 mm/h with $D_{eff} = 1.5 \times 10^{-9}\,\text{m}^2\,\text{s}^{-1}$. (*c*) No

699　dissolution, $D_{eff} = 1.7 \times 10^{-9}\,\text{m}^2\,\text{s}^{-1}$. Dashed lines denote simulated pH profiles, while

700　dotted lines show the pH profiles calculated assuming that the experimental

701　fluorescence decrease is caused solely by the effect of pH on α.
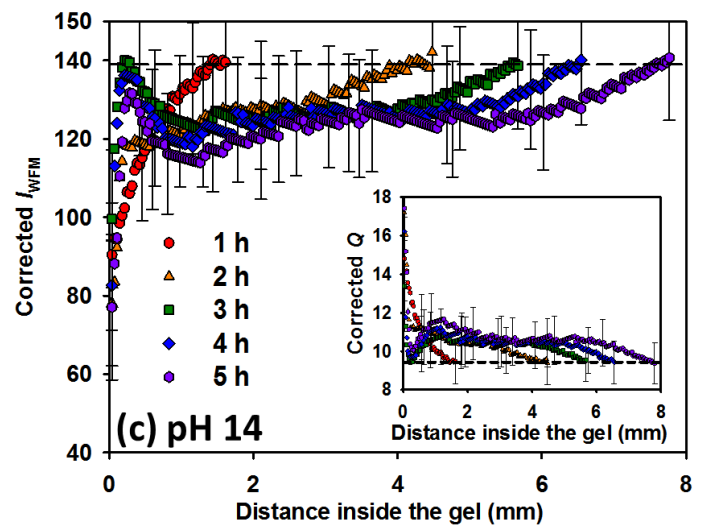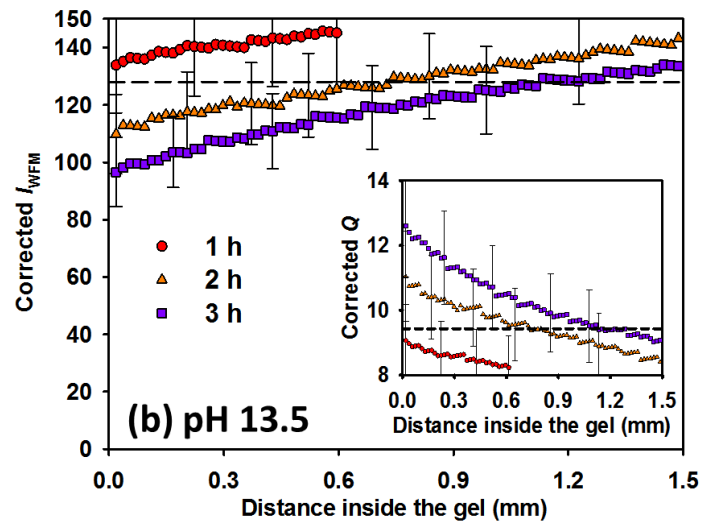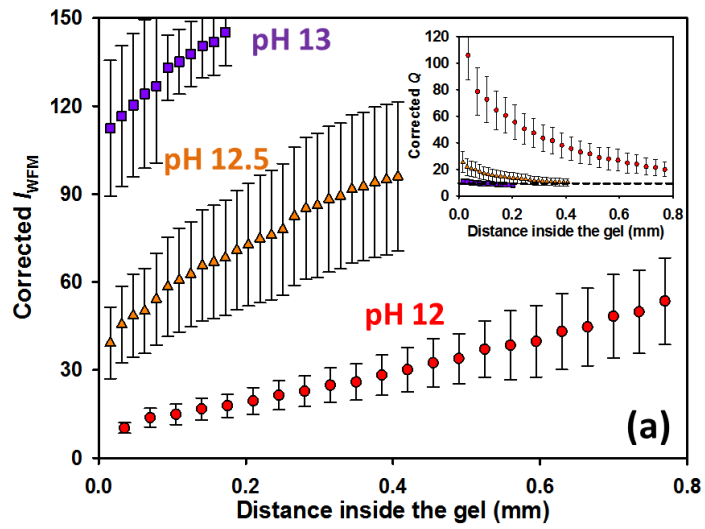
702

703

704 **Figure 13**. Corrected fluorescence intensity profiles for gels dissolving at pH (*a*) 12-

705 13, at steady state, and at different times at pH (*b*) 13.5 and (c) 14. Insets show the

706 corresponding swelling ratio profiles. The black dashed lines refer to the fluorescence

707 intensity or Q at formation ($Q_r = 9.43$). Error bars show uncertainty associated with

708 both the fluorescence intensity and α.

709
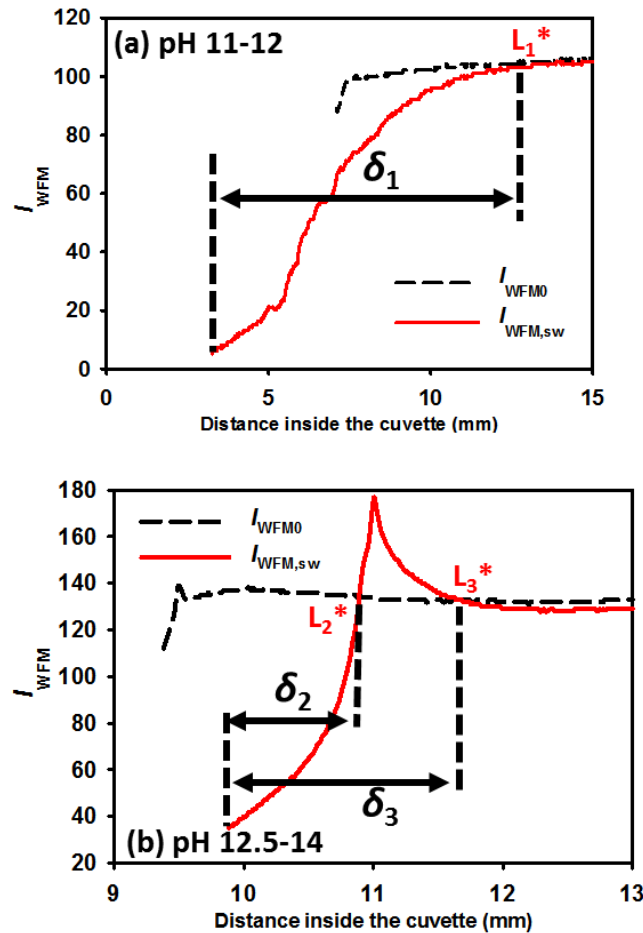
710

711

712 **Figure 14**. Schematics of measures of NaOH penetration depth based on uncorrected

713 fluorescence profiles. L_1^* is the location where the fluorescence intensity is the same

714 as the initial value using spline interpolation. In the cases when fluorescence peak exists,

715 L_2^* refers to the value ahead of the peak, while L_3^* denotes the value located after the

716 peak.
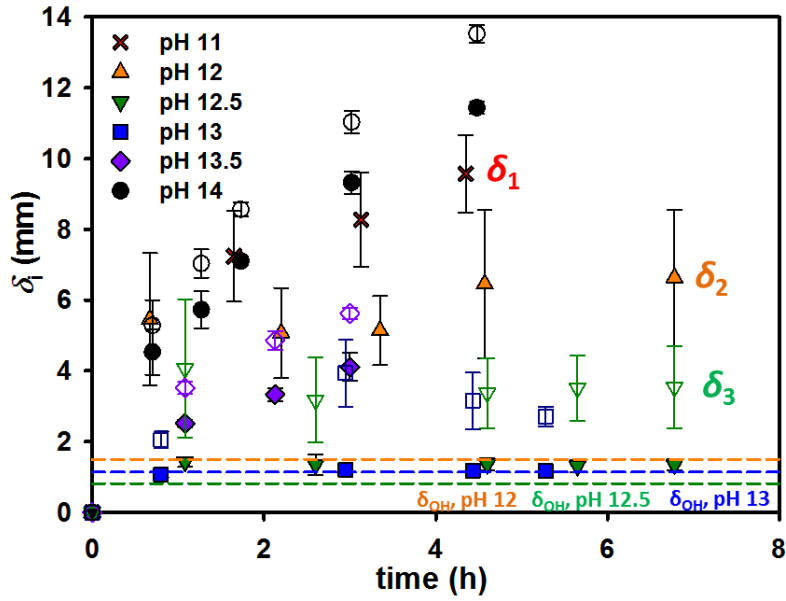
Figure 15. Evolution of estimated NaOH penetration depth for 15 wt% WPI-RITC gels at different pH (see legend), where δ_i was estimated as described in Fig. 14. Error bars show SDs of triplicates. Colored horizontal dashed lines indicate the NaOH penetration depth, δ_{OH}, in BLG gels reported by Mercadé-Prieto et al. (2008a).

Table 1. Parameters obtained by regression fitting data sets in Fig. 11 to eq. (4)

[WPI] (wt%)	α_0	$\Delta\alpha$	p^*	Δp
0.75	0.69±0.04	-0.34±0.05	11.86±0.06	0.30±0.03
1.5	0.77±0.12	-0.45±0.14	11.81±0.17	0.21±0.09
5	0.76±0.07	-0.43±0.09	11.59±0.10	0.24±0.05
10†	0.84±0.11	-0.81±0.17	11.45±0.14	0.19±0.08
15	0.80±0.03	-0.55±0.06	11.21±0.04	0.22±0.02

† Data set not considered in subsequent fluorescence corrections.